Review of Scientific Instruments | ARTICLE | pubs.aip.org/aip/rsi

Determination of in-plane surface directions in scanning probe microscopy images

Cite as: Rev. Sci. Instrum. 95, 023702 (2024); doi: 10.1063/5.0182520
Submitted: 19 October 2023 • Accepted: 19 January 2024 •
Published Online: 12 February 2024

View Online

Export Citation

CrossMark

Bob Kyeyune,[a)] Reinhard Olbrich, Philipp Rahe, and Michael Reichling

AFFILIATIONS

Institut für Physik, Universität Osnabrück, Barbarastraße 7, 49076 Osnabrück, Germany

[a)]Author to whom correspondence should be addressed: bob.kyeyune@uos.de

ABSTRACT

We describe an approach to determine the in-plane crystallographic surface directions in scanning probe microscopy (SPM) images. This method is based on a one-time characterization of the SPM instrument with an appropriate test sample and is exemplified by the analysis of non-contact atomic force microscopy (NC-AFM) images on surfaces whose natural cleavage occurs along {111} planes. We introduce a two-dimensional rotation matrix relating the crystallographic surface directions known from an analysis of the macroscopic crystal to the directions in the NC-AFM images. The procedure takes into account rotations and mirror axes resulting from sample mounting, the SPM scanner rotation, the choice of scan direction, as well as data processing, storage, and display. We demonstrate the practicability of the approach by determining the $[11\bar{2}]$ direction in topographic images of a $CeO_2(111)$ film grown on a Si(111) wafer and atomic resolution images of $CaF_2(111)$ with an instrument based on the beetle-type scanner.

Published under an exclusive license by AIP Publishing. https://doi.org/10.1063/5.0182520

16 February 2024 09:37:16

I. INTRODUCTION

The knowledge of in-plane crystallographic surface directions is important for the characterization of surface features and processes. However, the unambiguous identification of a crystallographic surface direction in a scanning probe microscopy (SPM) image is often not straightforward. This issue, for instance, arises for crystals with the fluorite structure, where the symmetry properties of the topmost surface atomic layer are different from those of the surface triple layer. Here, we introduce a generally applicable method for determining the in-plane crystallographic surface directions in SPM images and exemplify the procedure by imaging (111) surfaces of crystals with the fluorite structure, namely CaF_2 and CeO_2, with non-contact atomic force microscopy (NC-AFM). These surfaces exhibit triple-layer steps with two types of orientation categorized as type I steps descending in the $\langle 11\bar{2}\rangle$ direction and type II descending in the $\langle \bar{1}\bar{1}2\rangle$ direction.[1,2] For both materials, it has been shown that type I and type II step edges can be distinguished by their different potential,[1,3] principally offering a possibility to determine the surface directions if the suitable experimental setup is available.

However, here, we choose an alternative path to determine the in-plane crystallographic surface directions in SPM images. The key aspect to this path is to retrieve the instrumental transfer function for determination of the in-plane crystallographic surface directions in the displayed SPM image. In addition, we characterize the in-plane crystallographic surface directions on a macroscopic fluorite-type crystal by analyzing {111} cleavage planes having a non-zero angle with respect to the (111) surface plane. We define the cleaved surface, a member of the {111} cleavage family of a bulk CaF_2 crystal, as the (111) plane and explore its atomic structure. We further investigate a CeO_2 film grown with a hex-Pr_2O_3 buffer layer on Si(111) that exhibits pyramid-like structures with a triangular base, whereby the vertices of the triangles are oriented in the $\langle \bar{1}\bar{1}2\rangle$ direction.[4,5] The pyramids are the result of the thermodynamic and kinetic conditions during growth[6] and resemble the threefold symmetry of the {111} surfaces imposed by the atomic structure of the uppermost O–Ce–O triple layer. Therefore, they are well suited for identifying surface directions as their registry with the Si substrate is known.[7] Cleaving the Si substrate of the CeO_2 film as well as cleaving the CaF_2 crystal allows the unambiguous determination of in-plane directions,[8] and this is used to verify the results presented here. While the cleaving method allows for the determination of crystallographic surface directions for the special samples described above, it is not applicable to other surfaces. In such cases, crystallographic surface directions can only be determined with the help of the orientation

Published under an exclusive license by AIP Publishing

of the macroscopic crystal as determined by the X-ray diffraction analysis and other means such as optical analysis for birefringent crystals.[9]

Here, we determine the instrumental transfer function for a beetle-type SPM where the coarse approach is intrinsically coupled to a rotation of the scan head. For both of our test samples, crystallographic surface directions are known from X-ray diffraction in conjunction with cleaving along a plane different from the surface plane. We derive a two-dimensional rotational matrix transforming an arbitrary crystallographic surface direction into a direction in the displayed SPM image. The matrix depends on system rotations such as the direction in the sample surface coordinate system, sample mount, scanner rotation, and scan angle. Our approach is universal and can be applied to any scanning probe measurement. For the implementation, it is important to identify and verify all relevant rotations and mirror operations for the respective instrument. In SPM images produced by an instrument calibrated in this way, a certain in-plane crystallographic direction can easily be marked, provided one in-plane direction is known for the macroscopic crystal under investigation.

For our experiments, we use the RHK (Troy, MI USA) beetle-type UHV VT STM/AFM UHV750 system operated in ultra-high vacuum at room temperature with the R9 controller. We use two NANOSENSORS (Neuchatel, Switzerland) PPP-NCH silicon cantilevers having eigenfrequencies f_0 = 304.409 kHz and f_0 = 306.036 kHz, with quality factors Q = 35 000 and Q = 22 000, respectively. The tips are cleaned by Ar^+ ion sputtering. Images of the CeO_2 film are acquired in the topography mode (constant Δf mode), where a feedback system regulates the tip–sample distance to maintain a constant frequency shift Δf. The oscillation amplitude of the cantilever is 7.4 nm. Atomic resolution measurements on $CaF_2(111)$ are acquired in the quasi-constant height mode.[10] The symmetric design of the beetle scanner compensates for most of the first-order drift; however, for long time series of imaging, residual drift may affect imaging. Therefore, an atom tracking system with a feed-forward routine is used to compensate for thermal drift during scanning.[11]

II. APPROACH

We consider a rectangular sample and define an arbitrary crystallographic surface direction via the unit length vector $\vec{V_s}$ related to sample surface coordinates (x_s, y_s) in the *sample coordinate system*. This coordinate system is defined by Euclidean space basis vectors $\hat{e}_{x,s}$ and $\hat{e}_{y,s}$ as illustrated in Fig. 1(a). In particular, we define $\vec{V_s}$ through a counterclockwise rotation of the unit vector $\hat{e}_{x,s}$ by an angle Ω, namely,

$$\vec{V_s} = \begin{pmatrix} \cos\Omega & -\sin\Omega \\ \sin\Omega & \cos\Omega \end{pmatrix} \hat{e}_{x,s}. \quad (1)$$

Figures 1(b)–1(d) define the three transformations between coordinate systems related to SPM imaging experiments as discussed in the following: the sample rotation angle Λ defined by the orientation of the sample relative to the sample holder, the scanner rotation angle Θ describing how much the cantilever is rotated from its resting position, and the scan angle Ψ defining the angle of the fast scan direction relative to the cantilever coordinate axes. Note that the origin of all coordinate systems depicted in Fig. 1(b) is the origin of the $\hat{e}_{x,s}$, $\hat{e}_{y,s}$ coordinate system and all coordinates are rendered positive in the directions of the arrows describing the coordinate axes. The coordinate systems are drawn with different origins for better clarity.

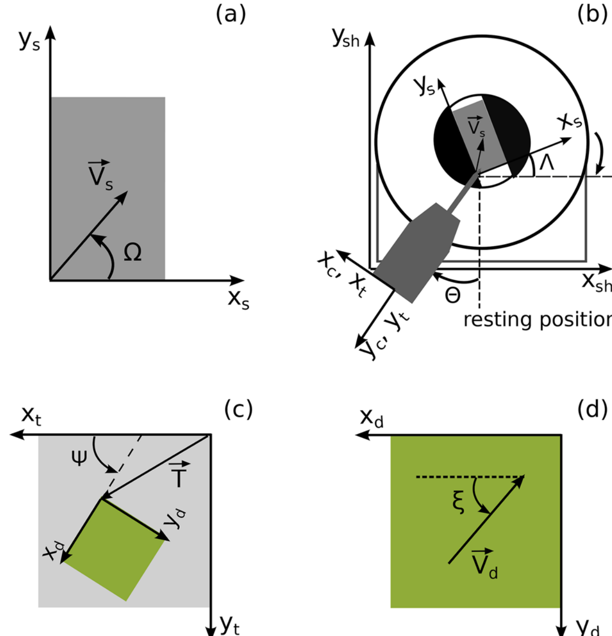

FIG. 1. Definition of coordinate systems and rotation angles: (a) Sample surface (gray area) with sample coordinates x_s and y_s. Ω is the angle between the crystallographic surface unit vector $\vec{V_s}$ and the $\hat{e}_{x,s}$ vector. (b) The sample is inserted in the sample-holder at an angle Λ relative to the sample-holder $\hat{e}_{x,sh}$ vector. The tip coarse approach involves a scan head rotation by the angle Θ relating the cantilever and sample holder coordinate systems. The coordinates x_c and y_c describe the sample coordinates after the tip approach, while x_t and y_t describe the tip movements during scanning. (c) Scan window (gray) and scan area (green) indicating the tip movement depending on the scan angle Ψ. x_d and y_d are the coordinates of the displayed image. For better clarity, coordinate systems in panel (b) and $\vec{V_d}$ in panel (d) are drawn with an arbitrary offset to the origin.

Figure 1(b) illustrates the coordinate system of the sample relative to the *sample holder coordinate system* ($\hat{e}_{x,sh}$, $\hat{e}_{y,sh}$). The angle Λ results from the details of mounting the sample. The clockwise rotation of the sample surface coordinates by the angle Λ yields the sample holder coordinates (x_{sh}, y_{sh}),

$$\begin{pmatrix} x_{sh} \\ y_{sh} \end{pmatrix} = \begin{pmatrix} \cos\Lambda & \sin\Lambda \\ -\sin\Lambda & \cos\Lambda \end{pmatrix} \begin{pmatrix} x_s \\ y_s \end{pmatrix}. \quad (2)$$

Upon coarse approach, the beetle-type scan head makes a clockwise rotation Θ (see Fig. 2) until the tip reaches the desired tip–sample distance. When the scanner makes the rotation Θ, the *cantilever coordinate system* ($\hat{e}_{x,c}$, $\hat{e}_{y,c}$) makes an equivalent clockwise rotation relative to the sample holder system as illustrated in Fig. 1(b). To measure Θ, we engraved angle-marks in the sample holder as

16 February 2024 09:37:16

Published under an exclusive license by AIP Publishing

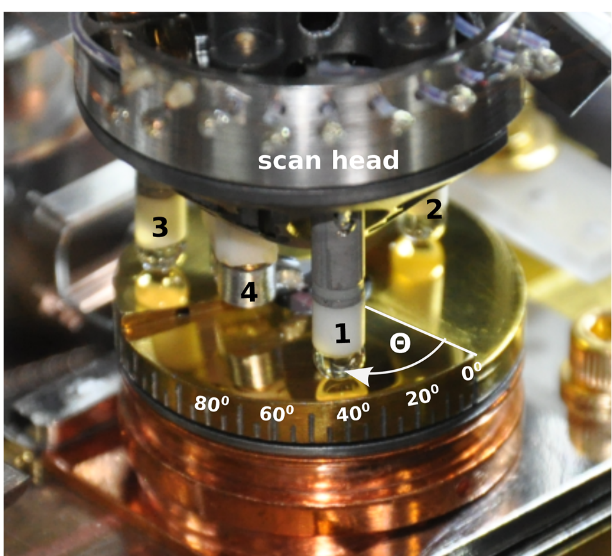

FIG. 2. Scan head and angle-marked sample holder of the beetle-type SPM allowing to determine the scan head rotation angle Θ. Piezo legs 1, 2, and 3 mark the rotation Θ relative to one of the three equivalent ramp edges. The scan head rotation directly translates into the rotation of the cantilever holder 4. The engraved angle marks are a home-made realization conducted in a mechanical workshop.

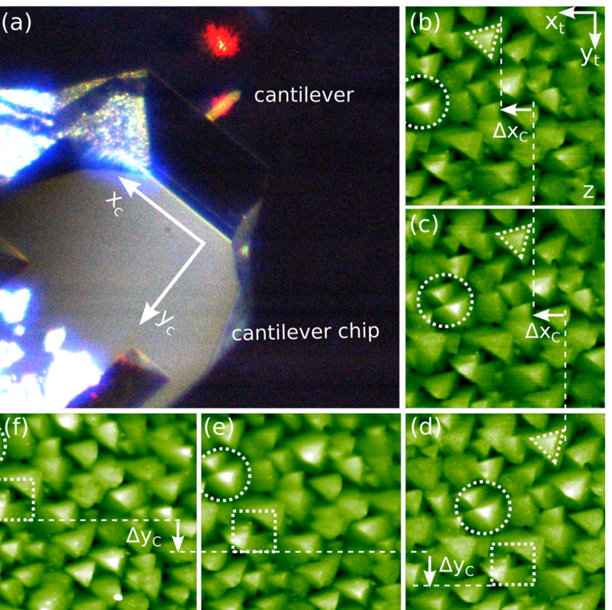

FIG. 3. (a) Optical micrograph obtained from a CCD camera observing cantilever coarse movements along the $\hat{e}_{x,c}$ and $\hat{e}_{y,c}$ vectors. (b)–(f) NC-AFM topographic images of the ceria film surface. Panels (c) to (d) are acquired after the tip having made coarse movements, resulting in a shift Δx_c in the positive $\hat{e}_{x,t}$ direction. Consequently, reference features enclosed in circles and triangles move opposite in the images. Panels (e)–(f) are acquired after the tip having made further coarse movements, resulting in shift Δy_c and Δx_c, in the positive $\hat{e}_{y,t}$ and negative $\hat{e}_{x,t}$ directions, respectively. Consequently, the features move up and left in the images.

depicted in Fig. 2 and observe the scan head movement using a CCD camera.

Figure 1(b) also describes the tip coarse movement in the directions $\hat{e}_{x,c}$ and $\hat{e}_{y,c}$ of the cantilever, while Fig. 3(a) demonstrates that we can follow sufficiently large coarse movement relative to the sample holder coordinates by visual inspection using a CCD camera. For the description of the transfer function, we need to identify the fast and slow scan directions of the tip and introduce the *tip coordinate system* ($\hat{e}_{x,t}$, $\hat{e}_{y,t}$). To establish a relationship between the coarse movement coordinates (x_c, y_c) and tip coordinates (x_t, y_t), we study the effect of the cantilever coarse movement on topographic images of the CeO_2 film. We first image the $500 \times 500\ nm^2$ area shown in Fig. 3(b), retract the tip, and then apply a single step coarse movement Δx_c in the positive $\hat{e}_{x,c}$ direction. The image taken at the new position is shown as Fig. 3(c), while Fig. 3(d) represents the image after a second single coarse step in the positive $\hat{e}_{x,c}$ direction. From the shift of the marked surface features, it is straightforward to conclude that the positive $\hat{e}_{x,c}$ direction is the same as the $\hat{e}_{x,t}$ direction, that is, the fast scanning direction. The procedure is repeated for a combination of two single step coarse movements Δy_c in the positive $\hat{e}_{y,c}$ direction with a movement in the $\hat{e}_{x,c}$ direction, yielding images shown in Figs. 3(e) and 3(f), respectively. Following the shift of marked features, we conclude that also for the slow scanning direction, there is an alignment between $\hat{e}_{y,c}$ and $\hat{e}_{y,t}$.

Consequently, we define the tip coordinates through a clockwise rotation of the sample holder system coordinates by the angle Θ as illustrated in Fig. 2,

$$\begin{pmatrix} x_t \\ y_t \end{pmatrix} = \begin{pmatrix} 1 & 0 \\ 0 & 1 \end{pmatrix} \begin{pmatrix} x_c \\ y_c \end{pmatrix} = -\begin{pmatrix} 1 & 0 \\ 0 & 1 \end{pmatrix} \begin{pmatrix} \cos\Theta & \sin\Theta \\ -\sin\Theta & \cos\Theta \end{pmatrix} \begin{pmatrix} x_{sh} \\ y_{sh} \end{pmatrix}. \tag{3}$$

The unity matrix in Eq. (3) indicates the identity of tip and cantilever coordinate systems in the present setup. Note that this matrix would have to be adapted for a setup where coarse and fine motions are not perfectly aligned. The minus sign in Eq. (3) reflects that the tip moves opposite to the sample holder coordinates for $\Theta = 0^\circ$, which is a reasonable convention for the beetle-type scanner. By combining Eq. (2) with Eq. (3), we obtain Eq. (4), relating the tip coordinates relative to the sample coordinates, namely,

$$\begin{pmatrix} x_t \\ y_t \end{pmatrix} = -\begin{pmatrix} \cos\Theta & \sin\Theta \\ -\sin\Theta & \cos\Theta \end{pmatrix} \begin{pmatrix} \cos\Lambda & \sin\Lambda \\ -\sin\Lambda & \cos\Lambda \end{pmatrix} \begin{pmatrix} x_s \\ y_s \end{pmatrix}. \tag{4}$$

By software control, the scan directions of the tip can be rotated by the scan angle Ψ with respect to the ($\hat{e}_{x,t}$, $\hat{e}_{y,t}$) coordinate system, yielding the *display coordinate system* ($\hat{e}_{x,d}$, $\hat{e}_{y,d}$) as illustrated in Fig. 1(c). The selection of the scan area usually does not only involve a rotation but also a translation of the tip coordinate system with respect to the display coordinate system as indicated by the vector $\vec{T}$ in Fig. 1(c). As we are interested here in directions, we solely focus on the rotation transforming the unit vector $\hat{e}_t$ in the unit vector $\hat{e}_d$,

$$\hat{e}_d = \begin{pmatrix} \cos\Psi & -\sin\Psi \\ \sin\Psi & \cos\Psi \end{pmatrix} \hat{e}_t. \tag{5}$$

16 February 2024 09:37:16

Published under an exclusive license by AIP Publishing

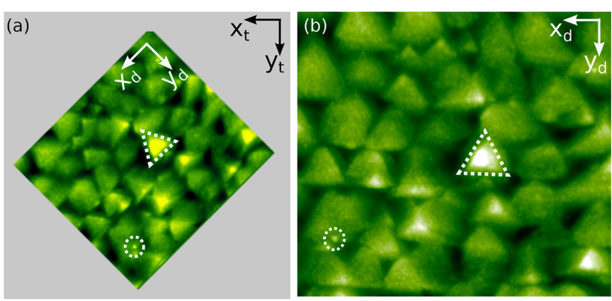

FIG. 4. (a) Scan window view indicating the display directions $\hat{e}_{x,d}$ and $\hat{e}_{y,d}$ at a scan angle of $\Psi = 45°$ with respect to the scanning directions $\hat{e}_{x,t}$ and $\hat{e}_{y,t}$. (b) Corresponding image displayed on the screen.

To experimentally verify this rotation, we perform a measurement of the CeO_2 film at an angle of $\Psi = 45°$. Figure 4(a) shows the area selection and rotation in the scan window of the R9 control software. The analysis software displays the scanned image as depicted in Fig. 4(b).

By combining Eqs. (4) and (5) with $(x_t, y_t) = \hat{e}_t$ and $(x_s, y_s) = \hat{e}_s$, we express the display coordinate unit vector $\hat{e}_d$ by the sample coordinate unit vector $\hat{e}_s$,

$$\hat{e}_d = -\begin{pmatrix} \cos\eta & -\sin\eta \\ \sin\eta & \cos\eta \end{pmatrix} \hat{e}_s, \tag{6}$$

where the angle η is given as $\eta = \Psi - \Theta - \Lambda$. The final step is to express the arbitrary unit length vector $\vec{V}_s$, which was defined in the crystallographic sample coordinate system as a vector $\vec{V}_d$, by the display coordinates. Inserting the inverse of Eq. (6) into Eq. (1) yields

$$\begin{aligned} \vec{V}_d &= -\begin{pmatrix} \cos\Omega & -\sin\Omega \\ \sin\Omega & \cos\Omega \end{pmatrix} \begin{pmatrix} \cos\eta & \sin\eta \\ -\sin\eta & \cos\eta \end{pmatrix} \hat{e}_{x,d} \\ &= -\begin{pmatrix} \cos\xi & -\sin\xi \\ \sin\xi & \cos\xi \end{pmatrix} \hat{e}_{x,d} \end{aligned} \tag{7}$$

with the angle

$$\xi = \Omega - \eta = \Omega - \Psi + \Theta + \Lambda. \tag{8}$$

This relation establishes how a given surface vector $\vec{V}_s$ in the sample coordinate system appears as $\vec{V}_d$ in the display coordinate system as illustrated in Fig. 1(d). Equation (7) implies that $\vec{V}_d$ is the result of a counterclockwise rotation of the unit vector $\hat{e}_{x,d}$ by ξ, while the minus sign in the equation inverts the tip coordinates at the origin. This equation is system specific for the beetle-type scanner but can be adapted to any SPM system by introducing appropriate rotations and mirror operations.

III. IMPLEMENTATION

To explore the practicability of the method, we choose the $[11\bar{2}]$ direction on the (111) surface of two samples as $\vec{V}_s$. The first sample is the hex-Pr_2O_3 buffered CeO_2 film deposited on a Si(111) substrate. The as-grown film exhibits characteristic pyramid-like structures with a well-defined orientation defining the $[11\bar{2}]$ direction. The second sample is a bulk CaF_2 crystal. The atomic resolution NC-AFM imaging on its (111) surface reveals a characteristic contrast pattern that also allows for a definition of the $[11\bar{2}]$ direction.[10,12]

To define $[11\bar{2}]$ on the macroscopic (111) surface, we adopt the cleavage method for crystals with a known crystal orientation of the bulk crystal and surfaces whose principal cleavage planes are $\{111\}$ planes as exemplified for a Si(111) wafer in Ref. 8. In our case, the sample to be cleaved is cut out from the Si(111) wafer by scribing vertical and horizontal lines on the aligned wafer using a diamond tipped cutter as illustrated in Fig. 5(a). When removing the cut sample from the wafer, we keep track of its orientation relative to the wafer flat by cutting one of its edges. By scribing the sample along $[1\bar{1}0]$, we produce $\{111\}$ planes different from the surface plane as illustrated in Fig. 5(b). The optical micrograph shown in Fig. 5(c) reveals two cleaved $\{111\}$ surfaces. The angle $\theta_{(hkl)}$ formed by the surface (hkl) with the (111) plane is given by[13]

$$\theta_{(hkl)} = \arccos\left(\frac{h+k+l}{\sqrt{3(h^2+k^2+l^2)}}\right). \tag{9}$$

The $\{111\}$ surfaces produced by cleaving and the surface directions $[11\bar{2}]$ and $[1\bar{1}0]$ are illustrated in Fig. 5(d). Furthermore, we notice the cleavage crack to propagate along $\langle 1\bar{1}0\rangle$ as earlier reported for single crystalline silicon.[14,15] We find that the planes $(\bar{1}\bar{1}1)$ and $(11\bar{1})$ form angles of $\beta = 70.53°$ and $\alpha = 109.47°$ with the (111) surface, respectively, in accordance with the experimental result shown in Fig. 5(c).

The first sample investigated by NC-AFM is a CeO_2 film. A 7×7 mm^2 sample is cut from the wafer following scribing and

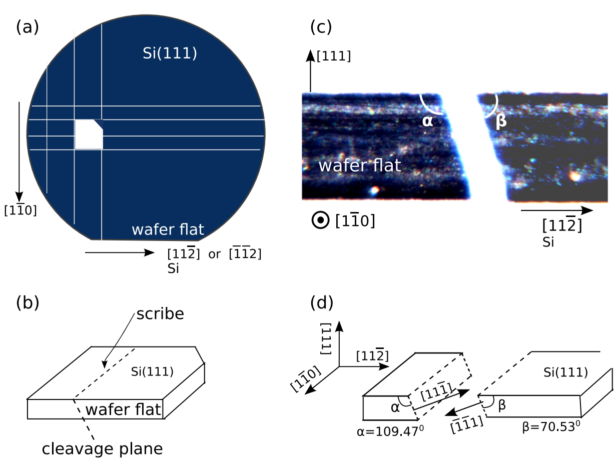

FIG. 5. Illustration of the cleaving method to determine the sample orientation. (a) Sample cut out from the Si (111) wafer. (b) Direction of the scribe on the sample. (c) Micrograph of two cleaved surfaces making angles of α and β with the (111) surface. (d) Definition of surface directions $[11\bar{2}]$ and $[1\bar{1}0]$ on the (111) surface, and the $[11\bar{1}]$ and $[\bar{1}\bar{1}1]$ planes produced by cleaving and the angles α and β.

16 February 2024 09:37:16

Published under an exclusive license by AIP Publishing

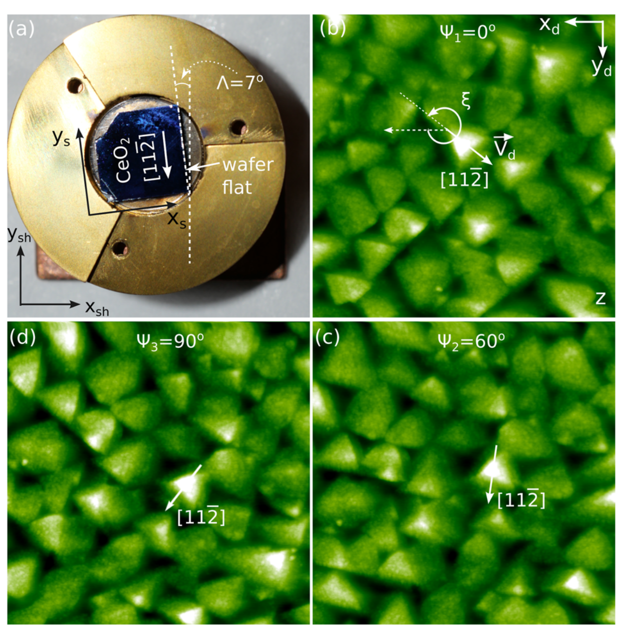

FIG. 6. (a) CeO_2 thin film on a Si(111) substrate mounted in the sample holder. The ceria $[11\bar{2}]$ direction is rotated by 180° relative to that of the silicon wafer. Therefore, CeO_2 $[11\bar{2}]$ expresses an angle of $\Omega = 270°$ relative to the x_s coordinate axis. (b), (c), and (d) are the NC-AFM topographic images scanned at scan angles $\Psi_i = 0°, 60°$, and 90°, respectively. The images represent the respective orientation of $[11\bar{2}]$ for $\Theta = 45°$.

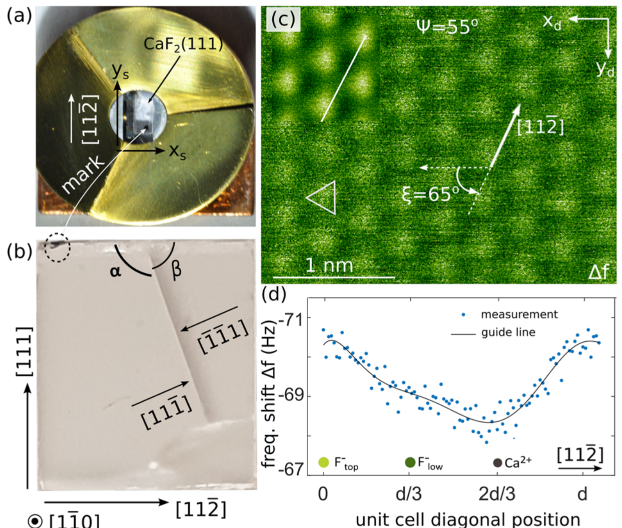

FIG. 7. (a) CaF_2 crystal with (111) surface orientation mounted in the sample holder with one corner marked by a black spot. (b) $\{111\}$ surfaces produced by cleaving the crystal a second time, for determination of the $[11\bar{2}]$ direction. (c) Atomic resolution image acquired in the quasi-constant height mode at $\Delta f = -69.2$ Hz with a positively terminated tip. The top-left inset is an extended unit cell average. (d) Frequency shift Δf along the averaged unit cell diagonal representing the $[11\bar{2}]$ direction. The solid line is a polynomial fit of degree seven through the data drawn as a guide to the eye. The length of the unit cell diagonal is $d = \sqrt{3}\,a$, where a is the lattice constant of the $CaF_2(111)$ surface.

cleaving as described above. The sample is inserted into the sample holder with $\Lambda = 7°$ as shown in Fig. 6(a). The coarse approach of the tip yields a scan head rotation of $\Theta = 45°$. The topographic images in Figs. 6(b)–6(d) are acquired at scan angles $\Psi_i = 0°, 60°$, and 90°, respectively. From the cleavage of the Si(111) wafer, we define the $[11\bar{2}]$ direction on the $CeO_2(111)$ thin film sample as shown in Fig. 6(a). Note that the $[11\bar{2}]$ direction of $CeO_2(111)$ is rotated 180° relative to that of the Si(111) wafer as the ceria film grows twin-free in type-B epitaxy.[7] This means that all surface directions on the ceria film are rotated by 180° with respect to the Si(111) surface directions. Consequently, we define $\vec{V}_s = (0, -1)$, which leads to $\Omega = 270°$. Using Eq. (8), we find $\xi = 322°, 262°$, and 232° for the three scan angles Ψ_i. By employing the transfer function of Eq. (7), we obtain the orientation of the $[11\bar{2}]$ direction in the experimental images as shown in Figs. 6(b)–6(d). Indeed, we observe that triangular pyramid-like structures have the vertex oriented opposite the $[11\bar{2}]$ direction in accordance with previous studies on the CeO_2/Pr_2O_3/Si(111) system.[4,5] It should be noted that experimental conditions beyond thermal drift such as creep could cause a deviation between the deduced orientations relative to the observed surface features. We estimate an experimental uncertainty of ±2.5° for measured angles Θ.

The second sample investigated is a cuboid $CaF_2(111)$ crystal aligned parallel to the sample holder coordinate system, thus $\Lambda = 0°$ as shown in Fig. 7(a). From the X-ray analysis, it is known that the long edge is aligned with the $[\bar{1}\bar{1}2]$ and $[11\bar{2}]$ directions. The surface is cleaved in UHV to obtain a clean (111) surface, which is the natural cleavage plane.[16,17] The surface is approached for imaging with a scan head rotation of $\Theta = 30°$. The atomic resolution NC-AFM image in Fig. 7(c) is acquired at scan angle of $\Psi = 55°$. After the experiment, the crystal is taken out of the UHV chamber to define the $[11\bar{2}]$ direction by the $\{111\}$ surface cleavage method. With the crystal still in the sample holder, we mark the crystal at a corner with a pen [see Fig. 7(a)] to keep track of the orientation of the sample in the sample holder system. After the removal of the crystal from the sample holder, the crystal is scratched along a $[1\bar{1}0]$ direction (parallel to the short edge). The cleaving is illustrated in Fig. 7(b), and the $[11\bar{2}]$ surface direction is found from the cleavage geometry as marked in Fig. 7(a). From Figs. 7(a) and 7(b), we deduce that the $[11\bar{2}]$ direction forms an angle of $\Omega = 90°$ with $\hat{e}_{x,s}$, yielding $\xi = 65°$ from Eq. (8). With the rotation transfer function, we mark the orientation of $[11\bar{2}]$ in the atomic resolution image shown in Fig. 7(c). Figure 7(d) shows the Δf contrast profile along the diagonal of the averaged unit cell (upper left inset in Fig. 7(c)) along the $[11\bar{2}]$ direction. The profile can be ascribed to images with a triangular contrast pattern,[10,12,18] as marked in Fig. 7(c). The triangles point in the $[11\bar{2}]$ direction in accordance with earlier studies on contrast formation on $CaF_2(111)$ for a positively terminated tip.[10,12] By analyzing the line profile associated with the triangular pattern, we identify the sub-lattices F^-_{top}, F^-_{low}, and Ca^{2+}, which are the fluorine ions in the top layer and the third layer and the calcium ion in the second layer of the $CaF_2(111)$ surface, respectively.

16 February 2024 09:37:16

Published under an exclusive license by AIP Publishing

IV. CONCLUSION

We introduced a method to unambiguously determine the orientation of in-plane surface directions in SPM images based on a rotation matrix that describes the instrumental transfer function and demonstrated the feasibility of the method for a beetle-type SPM. This approach can be used with any sample provided the orientation of one in-plane surface direction is known from an analysis of the macroscopic crystal. For surfaces whose natural cleavage planes are the $\{111\}$ surfaces, such as crystals possessing the fluorite or diamond structure, cleaving the crystal along non-parallel planes defines all surface directions. The important point in setting up the transformation matrix for deriving directions in the display coordinate system from directions in the sample coordinate system of the macroscopic crystal is to rigorously take into account all involved rotations and mirror operations. While this is straightforward for mechanical movements that can directly be observed, determining the fast and slow directions in SPM measurements and transformations introduced by the image acquisition and analysis software requires a careful analysis as the respective transformations are often not well documented. Once the transformation matrix has been defined, a simple computer script can be used to determine the orientation of any crystallographic surface direction in the SPM image from the knowledge of one crystallographic surface direction of the crystal under investigation.

AUTHOR DECLARATIONS

Conflict of Interest

The authors have no conflicts to disclose.

Author Contributions

Bob Kyeyune: Conceptualization (lead); Data curation (lead); Writing – original draft (lead); Writing – review & editing (lead). **Reinhard Olbrich**: Conceptualization (equal); Data curation (supporting); Writing – review & editing (equal). **Philipp Rahe**: Conceptualization (supporting); Writing – review & editing (equal). **Michael Reichling**: Conceptualization (lead); Writing – review & editing (lead).

DATA AVAILABILITY

The data that support the findings of this study are available from the corresponding author upon reasonable request.

REFERENCES

[1] H. H. Pieper, C. Barth, and M. Reichling, "Characterization of atomic step structures on $CaF_2(111)$ by their electric potential," Appl. Phys. Lett. **101**, 051601 (2012).
[2] S. Torbrügge, M. Cranney, and M. Reichling, "Morphology of step structures on $CeO_2(111)$," Appl. Phys. Lett. **93**, 073112 (2008).
[3] H. H. Pieper, C. Derks, M. H. Zoellner, R. Olbrich, L. Tröger, T. Schroeder, M. Neumann, and M. Reichling, "Morphology and nanostructure of $CeO_2(111)$ surfaces of single crystals and Si(111) supported ceria films," Phys. Chem. Chem. Phys. **14**, 15361–15368 (2012).
[4] R. Olbrich, H. Pieper, R. Oelke, H. Wilkens, J. Wollschläger, M. H. Zoellner, T. Schroeder, and M. Reichling, "A well-structured metastable ceria surface," Appl. Phys. Lett. **104**, 081910 (2014).
[5] In the NC-AFM image of Fig. 1 of Ref. 4, the $[\bar{1}\bar{1}2]$ is indicated correctly, however, the explanations given in the related paragraph and in the summary of Ref. 4 are misleading. For a detailed discussion of growth on a (111) surface of a face-centered cubic crystal see Ref. 6.
[6] J. Jacobsen, K. W. Jacobsen, and J. K. Norskov, "Island shapes in homoepitaxial growth of Pt(111)," Surf. Sci. **359**, 37–44 (1996).
[7] M. H. Zoellner, J. Dabrowski, P. Zaumseil, A. Giussani, M. A. Schubert, G. Lupina, H. Wilkens, J. Wollschläger, M. Reichling, M. Bäumer, and T. Schroeder, "Stacking behavior of twin-free type-B oriented $CeO_2(111)$ films on hexagonal $Pr_2O_3(0001)$/Si(111) systems," Phys. Rev. B **85**, 035302 (2012).
[8] W. Paul, Y. Miyahara, and P. H. Grütter, "Simple Si(111) surface preparation by thin wafer cleavage," J. Vac. Sci. Technol., A **31**, 023201 (2013).
[9] S. Kuhn, M. Kittelmann, Y. Sugimoto, M. Abe, A. Kühnle, and P. Rahe, "Identifying the absolute orientation of a low-symmetry surface in real space," Phys. Rev. B **90**, 195405 (2014).
[10] C. Barth, A. S. Foster, M. Reichling, and A. L. Shluger, "Contrast formation in atomic resolution scanning force microscopy on $CaF_2(111)$: Experiment and theory," J. Phys.: Condens. Matter **13**, 2061–2079 (2001).
[11] P. Rahe, J. Schütte, W. Schniederberend, M. Reichling, M. Abe, Y. Sugimoto, and A. Kühnle, "Flexible drift-compensation system for precise 3D force mapping in severe drift environments," Rev. Sci. Instrum. **82**, 063704 (2011).
[12] A. S. Foster, C. Barth, A. L. Shluger, and M. Reichling, "Unambiguous interpretation of atomically resolved force microscopy images of an insulator," Phys. Rev. Lett. **86**, 2373–2376 (2001).
[13] C. Tannous, "Crystal structure, X-ray diffraction and oblique geometry," Eur. J. Phys. **41**, 015501 (2019).
[14] R. Pérez and P. Gumbsch, "An *ab initio* study of the cleavage anisotropy in silicon," Acta Mater. **48**, 4517–4530 (2000).
[15] R. Pérez and P. Gumbsch, "Directional anisotropy in the cleavage fracture of silicon," Phys. Rev. Lett. **84**, 5347–5350 (2000).
[16] G. Benson and E. Dempsey, "The cohesive and surface energies of some crystals possessing the fluorite structure," Proc. R. Soc. London **266**, 344–358 (1962).
[17] L. Tröger, J. Schütte, F. Ostendorf, A. Kühnle, and M. Reichling, "Concept for support and cleavage of brittle crystals," Rev. Sci. Instrum. **80**, 063703 (2009).
[18] A. S. Foster, C. Barth, A. L. Shluger, R. M. Nieminen, and M. Reichling, "Role of tip structure and surface relaxation in atomic resolution dynamic force microscopy: $CaF_2(111)$ as a reference surface," Phys. Rev. B **66**, 235417 (2002).

16 February 2024 09:37:16

Published under an exclusive license by AIP Publishing